Site-Specific vs Specific Adsorption of Anions on Pt and Pt-Based Alloys

Maggie Teliska,[†,‡] Vivek S. Murthi,[§] Sanjeev Mukerjee,[§] and David E. Ramaker*[,†]

Chemistry Department, George Washington University, Washington, DC 20052, and Department of Chemistry and Chemical Biology, Northeastern University, Boston, Massachusetts 02115

Received: February 8, 2007; In Final Form: April 26, 2007

X-ray absorption spectroscopy (XAS) is utilized in situ to gain new insights into the electronic and chemical interactions of anions specifically adsorbed on Pt/C. A novel difference methodology was utilized, along with full-multiple scattering calculations using the FEFF8 code, to interpret the X-ray absorption near edge structure (XANES). Significant direct contact ("specific") anion adsorption occurs in 1 M H_2SO_4 and 6 M TFMSA, while it does not in 1 M $HClO_4$ and 1 M TFMSA. This specific anion adsorption significantly hinders O(H) chemisorption, particularly formation of subsurface O, causes the Pt nanoparticle to become more round, and weakens the Pt−Pt bonding at the surface. The specific anion adsorption becomes site-specific only after lateral interactions from other chemisorbed species such as OH on the surface force the anions to adsorb into specific sites. Alloying has a profound effect on the strength of the anion adsorption and whether site-specific or just specific adsorption occurs.

Introduction

The performance of many fuel cells is hindered by the high overvoltage in the oxygen reduction reaction (ORR). As previously discussed,[1] this can be attributed in part to formation of OH species chemisorbed on the electrode surface; however, other "specifically" adsorbed species such as anions from the electrolyte can also poison Pt sites.[2,3] The term specifically adsorbed here refers to those anions that are physisorbed or involved in some ionic or electrostatic interaction (as opposed to a chemical or covalent bond) via "direct contact" with the electrode surface. To become specifically adsorbed the anions have to displace first-row water molecules at that surface as opposed to only being localized in the water double layer next to the surface. In general, only anions (as opposed to cations) exist specifically absorbed on the surface.

Usually when the specifically adsorbed anion comes onto the electrode surface some small charge is transferred between the anion and the electrode to help form this ionic or electrostatic bond. Another term used in this work, "site-specific," refers to anions adsorbed in a specific site on the surface such as in an atop or 3-fold fcc Pt site. Specifically adsorbed anions may be site-specifically adsorbed or bound in random sites. It is generally not known whether specifically adsorbed anions are site-specifically adsorbed or not. All specific adsorption of anions, site-specifically adsorbed or not, has a profound effect on the Pt surface and kinetics of the ORR.

Development of new in situ and ex situ techniques has allowed the study of these specifically adsorbed anions on the electrode surface and provided some understanding of their influence on the chemical reactions taking place on that same surface.[4,5] That adsorbed anions influence the chemical reactions occurring on the same electrode surface has now been well documented.[6,7] For example, it is well known that the ORR rate is largely influenced by changes in the platinum surface structure, and this influence is often a result of anion adsorption or oxidation.[8] Specifically adsorbed anions also lower the fuel cell current densities by altering the hydrogen oxidation reaction at the anode.[9,10]

Specific Adsorption of (Bi)sulfate. Adsorption of (bi)sulfate [(bi)sulfate will be used to indicate bisulfate and/or sulfate anions] on metals immersed in sulfuric acid has been one of the most studied systems in electrochemistry.[11−14] Although many in situ and ex situ techniques have been used on both well-defined single-crystal and polycrystalline surfaces to study this adsorption, the geometry of the adsorbed (bi)sulfate and the effects of this adsorption on the Pt surface have been the subject of much debate.

Interest in (bi)sulfate adsorption on the Pt(111) electrode surface in sulfuric acid electrolyte arises in part from the cyclic voltammogram profile that shows a distinct peak called the "anomalous feature" or "butterfly" feature, which has been attributed to (bi)sulfate adsorption.[15−19] A number of studies have been devoted to determining the exact species (e.g., sulfate, bisulfate, bisulfate hydrogen bonded with OH) responsible for this feature, but clearly full agreement does not exist. On polycrystalline electrodes it has been generally found, based on CV profiles, that (bi)sulfate adsorbs preferably on steps and edges, the amount depending on the surface structure.[20−23] Most studies integrate the cyclic voltammograms to determine the total amount of charge density of adsorbed species; however, this method cannot distinguish between different anions (e.g., between SO_4^{2-} and HSO_4^-, which carry different ionic charge); it can only reflect the total charge density.[24,25] Others use chronocoloumetric data[26,27] to confirm some type of (bi)sulfate adsorption; however, no exact molecular identity or specific adsorption site has been determined from these studies.

Adsorption of (bi)sulfate on Pt electrode surfaces has also been studied on single-crystal systems in situ using infrared reflection-adsorption spectroscopy (IRAS) and Fourier transform infrared spectroscopy (FTIR), which are related techniques.[28−31]

* Author to whom correspondence should be addressed. Phone: (202) 994-6934. Fax: (202) 994-5873. E-mail: ramaker@gwu.edu.
† George Washington University.
‡ Current address: Johnson Controls Inc., 5757 North Green Bay Avenue, Milwaukee, WI 53207.
§ Northeastern University.

10.1021/jp071106k CCC: $37.00
Published on Web 06/12/2007

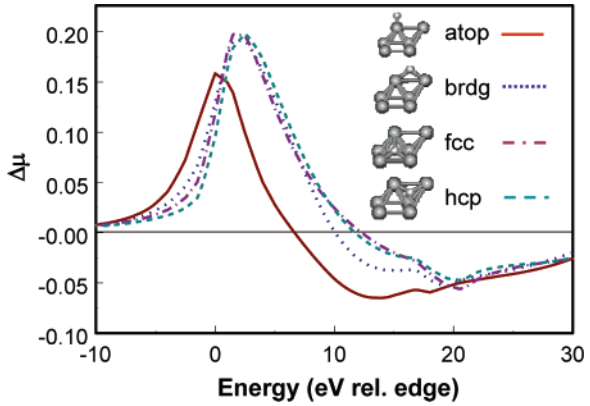

Figure 1. Theoretical $\Delta\mu = \mu(Pt_6Ox) - \mu(Pt_6)$ difference "signatures" obtained from the FEFF8 calculations on the clusters indicated.

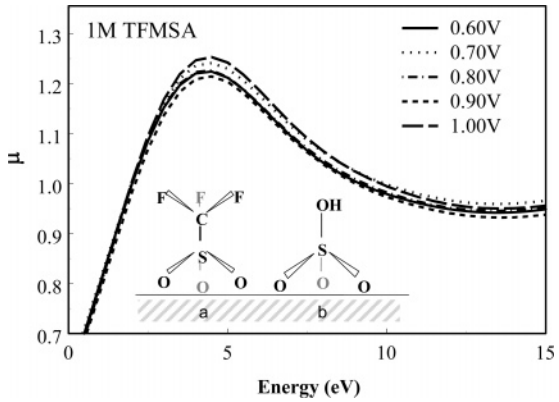

Figure 2. XANES data (μ) taken in 1 M TFMSA at the potentials indicated, normalized to one at 50 eV and on an energy scale relative to the bulk Pt edge. These spectra were carefully energy calibrated but otherwise not aligned or shifted. Specifically adsorbed TFMSA (a) and bisulfate (b) are illustrated.

Both IRAS and FTIR have shown that adsorption of (bi)sulfate species is strongly dependent on the structure of the electrode surface. For example, most agree that the (bi)sulfate adsorbs on Pt(111) via the three oxygens[32] (e.g., see inset of Figure 2), producing the single band observed at 1270 cm^{-1}, which is assigned to the SO_3 stretching mode for specific (bi)sulfate adsorption in the 3-fold sites.[33−36] On the other hand, studies on a Pt(100) surface show that the bisulfate prefers a 2-fold bridged coordination.[37]

The above conclusions are still somewhat controversial since there has been some disagreement in the assignments of the observed IR bands. Recently, Faguy et al. suggested that the adsorbed species producing the single band observed at 1270 cm^{-1} in the IRAS spectra was not that of (bi)sulfate but of a $H_3O^+-SO_3$ complex.[38,39] Further, Nart et al. concluded that this band arises from the S−O stretch of the noncoordinated SO bond of the adsorbed sulfate, and therefore, it could arise from either specifically or nonspecifically (i.e., in the OHP) adsorbed (bi)sulfate.[40] These inconsistent results point to the fact that there is no unambiguous in situ spectroscopic monitor of specific anion adsorption.

Radiotracer studies by Wieckowski[41−43] have provided the most straightforward evidence of the extent of (bi)sulfate adsorption. In these studies a radioactive isotope of S is used to label the (bi)sulfate with the magnitude of radioactivity coming off of a very thin layer at the surface then giving a measure of the adsorbed anions. These studies show that adsorption of (bi)sulfate is higher on Pt (111)[44] and Pt (100)[45] surfaces compared with Pt (110)[46] faces. Studies done on polycrystalline Pt[47] showed a decrease in the amount of adsorbed (bi)sulfate compared with single crystals. The magnitude of the adsorption is potential dependent on both polycrystalline and single-crystal faces and shows a maximum in the region where no other adsorbed species such as H, OH, and O are present. Results from these types of experiments will be given in the figures below.

Many other studies, however, do not agree with the results from radiotracer studies. For example, radiotracer studies show that the maximum adsorption of (bi)sulfate on a Pt(111) surface occurs around 0.6−0.8 V vs RHE.[48] Auger electron spectroscopy (AES) measurements show that the maximum adsorption falls at 0.92 vs RHE and that this is independent of the concentration of H_2SO_4 in solution.[49] In situ STM measurements show that $(\sqrt{3} \times \sqrt{7})$R19 structure disappears above 0.5−0.7 V; however, this may or may not indicate that the maximum adsorption occurs in this range.[50] In situ FTIR studies show the amount of (bi)sulfate increases all the way up to 1.4 V RHE;[34] however, SNIFTIRS (subtractively normalized interfacial FTIR spectroscopy) data show a decrease again at higher potentials.[51] Other techniques, including X-ray scattering, also confirm the presence of (bi)sulfate adsorption.[52,53]

Specific Adsorption of Perchlorate. Several workers have reported enhanced fuel cell activity when using $HClO_4$ over H_2SO_4 electrolyte and attribute this to loss of (bi)sulfate anion adsorption which blocks Pt sites for the ORR.[54,55] Several studies claim in fact to see adsorbed perchlorate ion; however, it is often confused with perchlorate ions in the water double-layer region since most agree that the perchlorate ion does not specifically adsorb and remains part of the water double layer.[56−62] This is confirmed by results which show that adding perchlorate ions to the electrolyte solution along with (bi)sulfate ions does not alter the amount of (bi)sulfate that specifically adsorbs.

It is unclear why (bi)sulfate specifically adsorbs and perchorlate does not, particularly since they are isoelectronic species. One proposed theory is that the sulfur in the (bi)sulfate has a higher "backdonation" than the chorine on the perchlorate ion. This backdonation arises from a lower HOMO−LUMO gap in the (bi)sulfate than in the perchlorate.[63] This mechanism is also suggested by core electron energy loss spectroscopy (EELS), which shows that the charge density around the sulfur atom is higher than with the chlorine. The lower charge density on the Cl was then used to explain the lower binding energy of the perchlorate compared to the bisulsulfate.

Direct Adsorption of TFMSA. It is well known that the current from phosphoric acid fuel cells (PAFC) is hindered by the high overvoltage of the ORR due in part to adsorption of phosphate anions at the electrode surface.[64] An early alternative was the use of fluoroalkane sulfonic acids as an electrolyte to alleviate the adsorption problems. Studies done using trifluoromethanesulfonic acid (TFMSA; see inset in Figure 2) as the electrolyte show an enhanced catalytic activity compared with phosphoric and even perchloric acid electrolytes.[65−67] The higher currents in TFMSA were attributed to better proton conductivity, higher oxygen solubility, and reduced specific anion adsorption compared with the more normal concentrated phosphoric acid electrolyte.[68] Radiotracer studies show much smaller adsorption of TFMSA compared with that in phosphoric acid.[68]

Studies using concentrated TFMSA electrolyte also show increased ORR activity and enhancement[69,70] compared to more dilute TFMSA.[71] The increased enhancement in concentrated TFMSA has been attributed to a lower water concentration as a consequence of protonation of most of the free water molecules

and therefore reduced adsorption of OH on the surface.[72] Reduction of OH on the surface in concentrated TFMSA has however not been directly observed spectroscopically.

In situ FTIR studies on polycrystalline Pt electrodes[73] in TFMSA electrolyte show a broad (1250−940 cm^{-1}) adsorption band only above 0.6 V vs RHE. Peaks in this band were assigned to the S−O asymmetric stretching mode and the S−O symmetric stretching mode. Adsorption bands at higher frequencies were attributed to the C−F bond vibrations. It has also been suggested that the F_3C end of the TFMSA could preferentially adsorb[74] on the Pt(111) faces; however, the F atoms may produce a strong repulsive interaction with the Pt atoms or steric hindrance,[75] and it is more likely that the SO_3 end adsorbs on the surface (as illustrated in Figure 2).

This Work. The objectives in this work are to determine (1) the potential dependence of the amount of O(H) and the effect of specifically adsorbed anions on this adsorption, (2) the effect of the adsorbed anion on the Pt catalyst, (3) the geometry and site preference of the site-specifically adsorbed anion, and (4) the role of adsorbed OH and its effect on site-specific anion adsorption.

Experimental Section

Electrocatalyst Preparation. The rather standard Pt/C electrode was studied along with two different carbon-supported binary alloys, PtFe/C and PtCo/C, with a nominal composition of 3:1 (Pt:M) atomic ratio. All electrocatalysts were prepared in house and had a metal loading of 20% on carbon support (Vulcan XC-72, Cabot). The preparation methodology used[76−79] was the well-known colloidal 'sol' and carbothermic reduction methods. Briefly, the preparation method involved initial preparation of a Pt/C sample using a sulfato complex approach described in more detail elsewhere.[80] Incorporation of the second alloying element was accomplished by first dispersing the supported electrocatalyst in an aqueous medium and raising the pH to 8 by addition of ammonium hydroxide. Next, the appropriate salt solution of the alloying element was added and the pH reduced to around 5, followed by drying and carbothermic reduction in an inert atmosphere at 900 °C. In these methods an oxide of the second alloying element is incorporated on the supported Pt/C electrocatalyst. When this is subjected to carbothermic reduction under inert conditions at 900 °C, the crystallites undergo reduction and alloying on the carbon support, thus providing for supported alloy nanoparticles.

TFMSA Electrolyte. The trifluoromethane sulfonic acid (TFMSA) was obtained from 3M Inc. and triply distilled under vacuum below 60 °C. The monohydrate (9.5 M) was then prepared from the purified acid. The pure white crystalline monohydrate was recrystallized two more times for further purification prior to preparation of the 6 and 1 M solutions used for this investigation. The solutions were first purged with N_2, and the electrode was cycled continuously until a clean reproducible Pt cyclic voltammetric profile was obtained. The solutions were then purged with O_2 for ORR measurements. The diffusion coefficient of oxygen and its solubility in these solutions were determined by a transient method using a Pt microelectrode as reported elsewhere.[81,82]

XAS Measurements. A special in situ spectroelectrochemical cell (described in detail elsewhere)[83] was used, which allowed XAS measurements in transmission mode with the working electrode in a fully flooded state. XAS measurements were conducted at beam line X-11 A at the National Synchrotron Light Source (NSLS) in Brookhaven National Laboratory with the storage ring operating at 2.8 GeV and a current between 350 and 120 mA. Data were collected at the Pt L_3 edge in the transmission mode using a three-detector set up measuring the incident, sample transmitted, and Pt foil transmitted light intensity. The Pt foil XAS spectrum provided accurate energy calibration and alignment of the edge positions. Details of the beam line optics and monochromator are given elsewhere. The electrochemical control of the interface was enabled by a digital potentiostat/galvanostat (PGSTSAT 30, Autolab, Echochemie, Brinkmann Instruments). In situ XAS measurements were obtained using 0.1 M $HClO_4$ or H_2SO_4 electrolyte along with the 1 and 6 M TFMSA electrolytes described above. Prior to acquiring the in situ XAS spectra electrodes were cycled at least 25 times between 0.0 and 1.2 V.

XANES Analysis. The XANES analysis procedure used here is similar to that used previously for isolation of the Pt−H, Pt−O, and Pt−OH scattering contributions[1,84−90] and for Pt−CO contributions[91,92] Only a brief summary of the technique is given here. To highlight the effects of adsorption on the surface, the experimental $\Delta\mu = \mu(\text{ads/Pt}) - \mu(\text{Pt})$ for the Pt L_3 edge is obtained by subtracting the L_3 edges from one another where the μ obtained at 0.54 V RHE in the corresponding electrolyte (unless otherwise noted) is used as the reference (i.e., μ(Pt)) in this work. At 0.54 V no H or O is expected on the surface, and in $HClO_4$ no specifically adsorbed ions are expected either as suggested above. In the other electrolytes specifically adsorbed ions may exist, as noted below.

All XANES spectra were carefully energy calibrated before subtraction by aligning the Pt foil reference spectra taken simultaneously at each potential and then shifting the sample spectra according to the foil data. This energy calibration eliminates any shifts do to drift of the photon beam, etc. Other than this careful energy calibration, the spectra were not aligned as done in some of our previous work for H,[84−88] although the procedure used here is comparable to that used for H and O adsorption on a Pt electrode.

FEFF Calculations. FEFF8 calculations were performed to interpret the $\Delta\mu$ spectra using a series of Pt_6 and Pt_6O_x clusters with the geometric configuration shown in Figure 1. This cluster geometry is preferred[93] because it contains both fcc and hcp sites as indicated, and we used it previously for H and O adsorption with success.[88,90] Thus, throughout this work the indicated Pt_6 cluster is utilized with the Pt−Pt distance at 2.77 Å.

The FEFF8 code performs ab initio self-consistent field, real-space, full mutiple scattering calculations.[94] The Hedin−Lundquist potential was used in this work to describe the Pt−O scattering following the work of Ankudinov et al.[94] and our previous work on Pt−H and Pt−O scattering.[84,86−90] The theoretical $\Delta\mu$ difference spectra are obtained by taking the difference $\Delta\mu = \mu(Pt_6Ox) - \mu(Pt_6)$, giving theoretical results exactly comparable to that obtained experimentally. Comparison of these theoretical results, obtained by placement of O in the atop, bridged, 3-fold fcc, or 4-fold hcp sites as shown in Figure 1, with the experimental results enables determination of the adsorption sites.

Results

FEFF8 Results. Figure 1 gives a summary of the FEFF8 calculations showing the different "signatures" for O adsorption in each adsorption site of the Pt clusters indicated. These signatures will be used to identify the adsorption of OH, O, and even bisulfate or TFMSA since it is believed that it is the O atoms in these anions that make contact with the electrode surface as illustrated in Figure 2. The $\Delta\mu$ signature for the

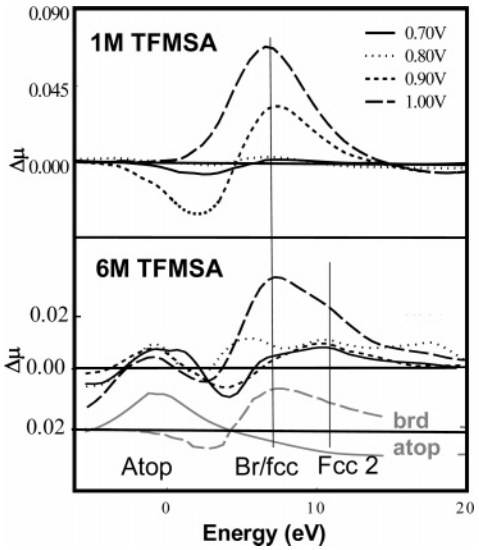

Figure 3. Difference spectra $\Delta\mu = \mu(V) - \mu(0.54\ \text{V})$ for a Pt/C electrode in 1 and 6 M TFMSA at the indicated potentials V relative to the RHE. Also shown is the optimally aligned FEFF8 theoretical signatures for O in an atop and brd/fcc binding sites.

different sites are similar; however, the $\Delta\mu$ signature for the atop O occurs at around 2−4 eV lower than that of the *n*-fold (bridge/fcc/hcp) bonded O, making it easy to distinguish the atop adsorption site. We have shown previously from DFT calculations[1] that OH prefers to be 1-fold coordinated while O prefers to be at least doubly coordinated to a Pt cluster. Thus, when the atop signature is seen, this is assigned to OH adsorption.

It should be noted that the theoretical signatures do change some with O coverage (i.e., x in the Pt_6O_x cluster), Pt−O bond length, and Pt_6 cluster geometry; thus, the signatures given in Figure 1 are representative only. In general, these theoretical signatures have to be shifted up by around 2−4 eV for optimal agreement with experiment. This occurs because the FEFF8 edge energy is not always in perfect agreement with experiment, and the edge in the experimental data and theory are not defined in exactly the same manner. Nevertheless, the O binding site appears to be the dominant factor, enabling determination of the coverage of both atop OH and *n*-fold O binding sites.

XANES Analysis. Figure 2 shows the typical XANES data (μ) taken in 1 M TFMSA at the potentials indicated. Although the differences with potential are quite small, they are clearly above the noise level, enabling meaningful differences, $\Delta\mu$, to be taken. Figure 3 shows the difference spectra, $\Delta\mu = \mu(\text{V}) - \mu(0.54)$, obtained by taking the indicated difference in the spectra shown in Figure 2 and similar data for 6 M TFMSA. It also compares these difference spectra with optimally aligned FEFF8 signatures from Figure 1 for the *n*-fold O adsorption sites. Clearly this shows that O(H) has adsorbed primarily in the *n*-fold sites on the Pt electrode at these potentials, as expected from previous work.

The results for 6 M TFMSA are remarkably different from those for 1 M TFMSA. We conclude that in 6 M TFMSA O adsorption occurs in both atop and bridge/fcc sites and a second fcc-like site appearing at slightly higher energy as indicated. The reason for this higher feature will be discussed below.

Discussion

Effect of (Bi)sulfate and TFMSA Adsorption on O(H) and H Adsorption. XANES results for Pt/C in 0.1 M $HClO_4$ and H_2SO_4 have been presented previously.[1,89,90] To highlight the

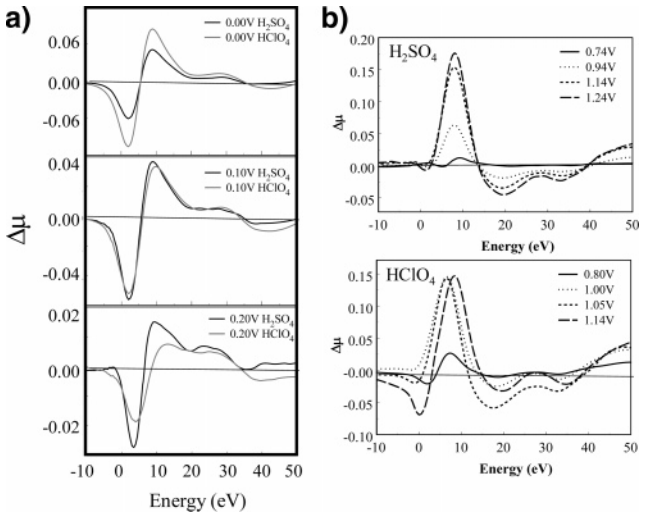

Figure 4. (a) Experimental $\Delta\mu = \mu(V) - \mu(0.54\ \text{V})$ difference spectra comparing H adsorption in both 0.1 M $HClO_4$ and H_2SO_4. The top, middle, and bottom spectra are for data at 0.0, 0.1, and 0.2 V vs RHE respectively. (b) Same for O adsorption in 0.1 M H_2SO_4 (top) and $HClO_4$ (bottom) at the indicated potentials.

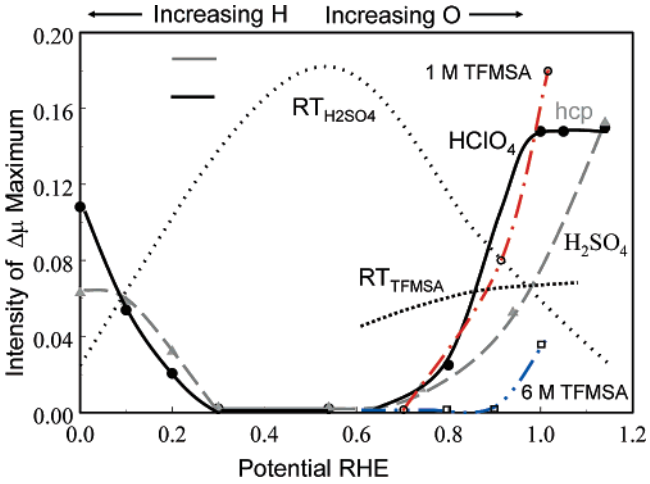

Figure 5. Radiotracer data (RT) showing direct adsorption of (bi)-sulfate[41,42] and TFMSA (in arbitrary units) along with the amounts of O(H) and H chemisorbed, as reflected in the amplitude of the $\Delta\mu$ maxima in Figures 3 and 4. The change in $\Delta\mu$ signature in $HClO_4$ to more like that of hcp/subsurface is discussed in the text.

effect of direct anion adsorption on chemisorption of O(H) and H, $\Delta\mu = \mu(\text{V}) - \mu(0.54)$ difference spectra are presented in Figure 4, making careful comparison between those in 0.1 M $HClO_4$ electrolyte and those in 0.1 M H_2SO_4. Figure 4 compares results taken at the same (or similar) potential with the same Pt/C electrode; only the electrolyte was changed. Clear differences in the magnitude of $\Delta\mu$ are visible; otherwise, the spectral shapes are remarkably similar. Differences in spectral shape were initially expected, reflecting the specifically adsorbed (bi)-sulfate anion in H_2SO_4 and its absence in $HClO_4$. As H or O(H) is adsorbed, some (bi)sulfate should be removed, and thus this effect should be visible. The absence of such differences suggest strongly that the specifically adsorbed (bi)sulfate are not seen in $\Delta\mu$ at all in this case. The reason for this will be discussed below.

To highlight the effects of the specifically adsorbed anions on chemisorption, Figure 5 shows the amplitude of $\Delta\mu$ at the maxima in Figures 3 and 4 vs the potential; this intensity reflects the amount of H or O(H) on the surface relative to that at 0.54 V, where we expect a "clean" surface. Figure 5 also shows

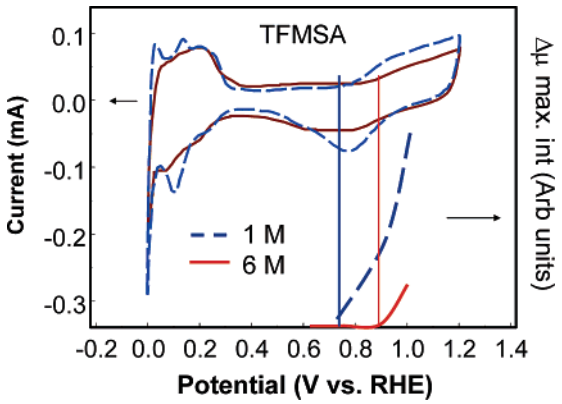

Figure 6. Current−voltage curves for 1 and 6 M TFMSA and comparison of the onsets with the corresponding $\Delta\mu$ curves in Figure 5.

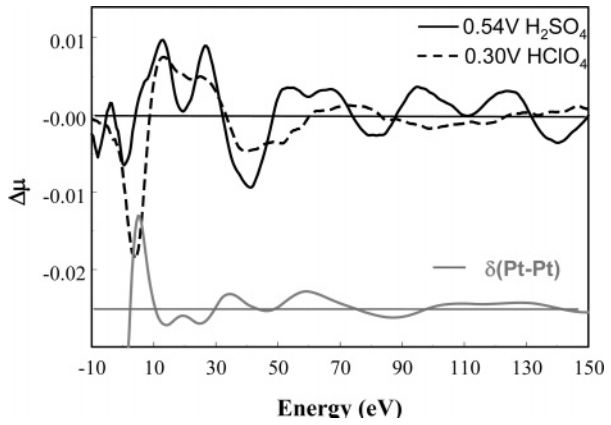

Figure 7. Comparison of the experimental $\Delta\mu = \mu(0.54\ \text{V}, H_2SO_4) - \mu(0.54\ \text{V}, HClO_4)$, reflecting the effect of specific (bi)sulfate adsorption, with $\Delta\mu = \mu(0.30\ \text{V}, HClO_4) - \mu(0.54\ \text{V}, HClO_4)$, reflecting the effect of delocalized H chemisorption, and with the Pt−Pt EXAFS scattering, $\delta(\text{Pt}-\text{Pt}) = x[\mu(0.54\ \text{V}, HClO_4) - 1]$, where x is chosen for convenience to fit on the same scale in this figure.

the change in amount of (bi)sulfate and TFMSA specifically adsorbed on the surface as reflected in recent radiotracer studies reported by Wieckowski et al.[41,42] and Zelanay et al.[73] These results clearly show the later onset for O(H) chemisorption in H_2SO_4 compared to that in $HClO_4$, a fact already discussed previously.[90,95] Further, although Figure 5 suggests that more O(H) is present in H_2SO_4 above 1.1 V, this is clearly not the case. The $\Delta\mu$ signature at 1.1 V in $HClO_4$ reflects that for hcp/subsurface O, while that in H_2SO_4 still reflects that of bridge/fcc O. The experimental $\Delta\mu$ signature for hcp/subsurface O is slightly broader with a smaller intensity at its maximum compared with the bridge/fcc signature (although not reflected in Figure 1), so that the plot in Figure 5 does not correctly reflect the relative amount of chemisorbed O(H) in this region.

Figure 5 also shows the dramatic affect that concentrated TFMSA electrolyte has on the O chemisorption, delaying onset until around 0.9 V RHE. Comparison of the onset for 1 M TFMSA with that for $HClO_4$ electrolyte reveals they have similar behavior. Thus, we conclude that in 1 M TFMSA little or no direct TFMSA anion adsorption occurs. It clearly occurs in the 6 M case however since it can be directly seen in the $\Delta\mu$ data, causing the peak around 12 eV in Figure 3, and this adsorption may be hindering the O chemisorption. Comparison of $\Delta\mu$ vs potential curve for 6 M TFMSA with that for 0.1 M H_2SO_4 in Figure 5 shows the onset in 6 M TFMSA to be more delayed, indicating that 6 M TFMSA electrolyte is much more effective at reducing O chemisorption compared with 0.1 M H_2SO_4 electrolyte. This probably occurs because of the reduced water concentration in 6 M TFMSA. Published ORR reactivities, found to be higher in 6 M TFMSA than in 1 M TFMSA, indeed suggest that the reduced OH poisoning in 6 M TFMSA due to reduced water concentration at the Pt surface has a larger positive effect on the ORR rate than the negative effect of the specifically adsorbed TFMSA anions.

Finally, Figure 6 compares the onset for OH adsorption visible in the $\Delta\mu$ amplitudes with current−voltage (CV) curves for 1 and 6 M TFMSA, showing good agreement.

The results for H chemisorption are also interesting since the $\Delta\mu$ data in Figure 5 show an earlier onset for H adsorption in H_2SO_4 but then at higher H coverage a decreased amount compared to that in $HClO_4$. These results can easily be explained when it is understood that the XANES $\Delta\mu$ reflects only the localized H on the surface. Previously, we showed that chemisorbed H does exist on the Pt surface in the region 3.0−0.45 V RHE but that this H is delocalized over the fcc/br/hcp sites so that it is not visible in the XANES scattering. As the surface becomes more covered with H, and hence lateral interactions become larger, this H is forced to localize into fcc sites. Figure 5 shows that the presence of the specifically adsorbed (bi)sulfate anions forces the H to localize into fcc sites at lower H coverage (when it becomes visible in the XANES $\Delta\mu$ data), apparently now because of lateral interactions between the (bi)sulfate and H atoms. At still higher H coverage however the (bi)sulfate apparently blocks adsorption of H, so lower coverage is seen. This is consistent with Figure 6, which shows that the chemisorbed TFMSA anions in 6 M TFMSA also changes the CV curves in the H adsorption region. The usual features at 0.1 and 0.25 V, due to H adsorption at the faces and edges/corners, respectively, are partially obscured in the presence of specifically adsorbed anions; indeed, the 0.1 V feature appears to be significantly reduced or least spread out over a range of potentials. This suggests that the stronger adsorbed H at the edges/corners is able to absorb unimpeded but the weaker adsorbed H on the faces is partially blocked due to specifically adsorbed anions. However, further work is required here to more fully confirm this.

Effect of Specifically Adsorbed Anions on Pt Nanoparticles. The specific or contact adsorption of anions not only strongly affects the chemisorption of H and O(H) but also it alters the shape of the Pt nanoparticles. To isolate this effect we take the XANES difference $\Delta\mu(0.54\ \text{V}\ H_2SO_4) = \mu(0.54\ \text{V}\ H_2SO_4) - \mu(0.54\ \text{V}\ HClO_4)$ in Figure 7. This difference should reflect only the effect of the specifically adsorbed (bi)sulfate anions because at 0.54 V O(H) chemisorption should be negligible. This spectral line shape is compared with $\Delta\mu(0.3\ \text{V}\ HClO_4) = \mu(0.3\ \text{V}, HClO_4) - \mu(0.54\ \text{V}, HClO_4)$, which we have shown previously reflects essentially the relaxation or change of the Pt−Pt bonding as a result of chemisorbed but

TABLE 1: Summary of Results for Different Electrolytes

electrolyte	0.54 V RHE	0.7(4) V RHE
1 M $HClO_4$	no adsorption	OH and O
1 M H_2SO_4	specific but not site-specific anion adsorption	OH plus site-specific anion adsorption
1 M TFMSA	little or no adsorption	OH and O
6 M TFMSA	specific but not site-specific anion adsorption	OH plus site-specific anion adsorption

delocalized H as discussed above. The scattering from H is not seen because it is delocalized (very large Debye−Waller factor), but the alteration of the Pt−Pt bonding resulting from this H adsorption shows up essentially as a component of Pt−Pt EXAFS scattering, δ(Pt−Pt), but 180° out of phase as shown in the figure. The similarity of the 0.54 V H_2SO_4 and 0.3 V $HClO_4$ spectral line shapes is quite striking below 50 eV. It indicates that the effect of the specific adsorption of bisulfate anion is nearly the same as delocalized H chemisorption. This suggests that direct scattering from specifically adsorbed (bi)-sulfate cannot be seen (because the anions are not adsorbed in registry with the Pt atoms on the surface, i.e., non-site-specifically adsorbed), but the effects of the anion adsorption weakens and/or changes the Pt−Pt bond near the surface just like for the delocalized H chemisorption.

Note that the agreement between these two difference spectra in Figure 7 occurs only below 50 eV. Above 50 eV, $\Delta\mu$(0.54 V, H_2SO_4) and $\Delta\mu$(0.54 V, $HClO_4$) are quite different; indeed, $\Delta\mu$(0.54 V, H_2SO_4) is now more in phase with the δ(Pt−Pt) EXAFS scattering as shown in the figure. Thus, the Pt−Pt scattering reflected in the $\Delta\mu$(0.54 V, H_2SO_4) difference spectrum is 180° out of phase with the normal EXAFS δ(Pt−Pt) scattering below 50 eV and nearly in phase with the δ(Pt−Pt) scattering well above 50 eV.

To understand this we need to consider the dominant contributions in each energy region. The region below 50 eV, where multiple scattering dominates, better reflects changes in the Pt−Pt electron distribution, and the region well above 50 eV, when single scattering dominates, reflects more the changes in Pt−Pt bond length. Thus, Figure 7 is consistent with a weakening of the surface Pt−Pt bonds due to (bi)sulfate adsorption causing the changes below 50 eV along with a change from a more oval- or pancake-like Pt nanoparticle to one which is more spherical, resulting in an increase in the single Pt−Pt scattering (or N_{Pt-Pt} coordination number) at higher energies. Previous studies of H/Pt nanoparticles have regularly shown that H adsorption results in elongation of the average Pt−Pt distance and an increase in Pt−Pt coordination number due to a more spherical nanoparticle shape after adsorption. It appears that specific (bi)sulfate adsorption does nearly the same thing.

We conclude from the XANES results above 50 eV that N_{Pt-Pt} is larger in the presence of specifically adsorbed anions because the Pt nanoparticles become more spherical to increase contact with the specifically adsorbed anions. The $\Delta\mu$(0.54 V, H_2SO_4) difference spectra below 50 eV suggest that the Pt−Pt bond distance also weakens and perhaps becomes slightly longer at the surface (the $\Delta\mu$ technique enhances surface effects by the difference approach). Clearly the specifically adsorbed (bi)-sulfate anions have a significant affect on the Pt nanoparticles.

Effect of Chemisorption and Alloys on Specific Anion Adsorption. The $\Delta\mu$ XANES results at 0.54 V RHE in Figure 7 reflect only changes in the Pt−Pt scattering; direct Pt−O scattering arising from specific adsorption of the (bi)-sulfate anions is not visible. This suggests that the (bi)sulfate anion adsorption, although specific, is not site specific because either the anions are mobile on the surface or they are adsorbed in random sites (i.e., they are not in registry with the Pt atoms at the surface), so that these O atoms do not show up in the XANES scattering. Table 1 organizes some of the conclusions regarding anion adsorption in the different electrolytes and at different potentials: the results at 0.54 V established thus far.

Table 1 indicates that the situation is entirely different at 0.7(4) V (0.74 V in H_2SO_4 and 0.7 V in TFMSA). To demonstrate this Figure 8 shows $\Delta\mu$ spectra at 0.7(4) V in 0.1 M H_2SO_4 and 6 M TFMSA. Both spectra show features from atop O(H) adsorption as well as fcc O adsorption. Previously we showed that the peak around 11−12 eV in $\Delta\mu$ arises from a long bonded O, which we attributed to the (bi)sulfate anions site-specifically adsorbed via the O atoms to the Pt in fcc sites. Thus, at 0.7(4) V in the presence of atop OH the (bi)sulfate and TFMSA anions apparently site-specifically adsorb so that the direct Pt−O scattering becomes visible. It seems clear that the lateral interactions from atop OH chemisorption now force the (bi)sulfate anions to localize or fill in some of the empty fcc sites in between the atop OH sites. In any event, they become visible in the XANES scattering only after some OH adsorption, and we can classify at least some of the specifically adsorbed anions as site-specifically adsorbed.

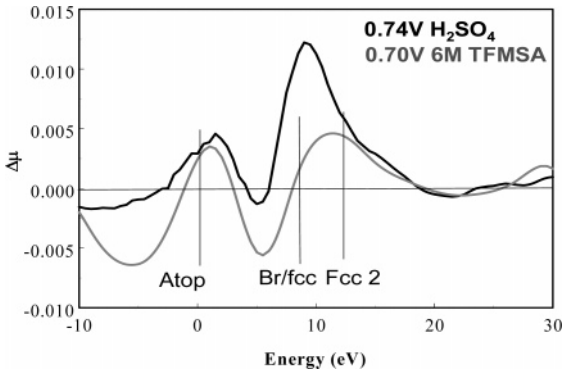

Figure 8. Comparison of $\Delta\mu$(0.74 V, H_2SO_4) = μ(0.74 V, H_2SO_4) − μ(0.54 V, $HClO_4$), reflecting the effects of (bi)sulfate adsorption, and μ(0.7 V, 6 M TFMSA) = μ(0.7 V, 6 M TFMSA) − μ(0.6 V, 1 M TFMSA), reflecting the effects of TFMSA "site-specific" anion adsorption.

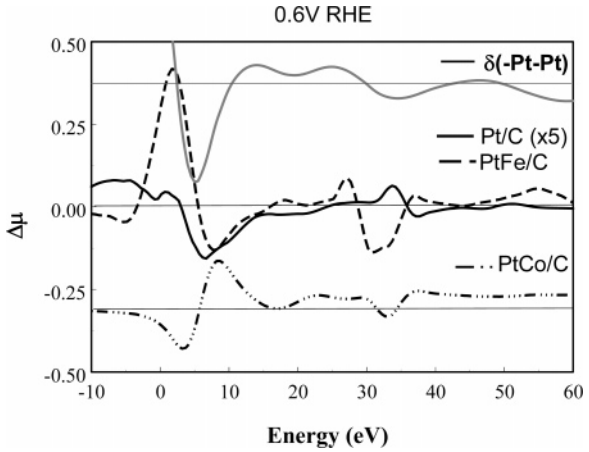

Figure 9. Experimental $\Delta\mu$ = μ(0.6 V, 6 M TFMSA) − μ(0.6 V, 1 M TFMSA) for Pt/C, Pt−Fe/C, and Pt−Co/C. Also shown is the −δ-(Pt−Pt) EXAFS scattering as discussed above.

Figure 9 shows the results of Pt−M (M = Co and Fe) alloying on anion adsorption. Figure 9 specifically compares $\Delta\mu$ = μ-(0.6 V, 6 M TFMSA) − μ(0.6 V, 1 M TFMSA) for Pt/C and two alloys, Pt_3Co/C and Pt_3Fe/C. At 0.6 V RHE little OH/Pt should exists, so this $\Delta\mu$ difference should isolate the effect of TMFSA anion adsorption. These alloys have been characterized previously by us[1] with EXAFS, XRD, and CV curves. The Pt_3-Co alloy has been shown to be more homogenously alloyed with both Pt and Co atoms at the surface and with the Co covered by O(H) at all potentials above 0.2 V. The Pt_3Fe alloy has a Pt skin at least two layers thick, so that no Fe atoms appear at the surface. Nevertheless, the subsurface Fe plays a critical role in modifying the OH adsorption behavior of the Pt surface via some electronic effect as described previously.

TABLE 2: Summary of TFMSA Results for Different Alloys

electrode	1 M TFMSA at 0.6 V RHE	6 M TFMSA at 0.6 V RHE
Pt/C	little anion adsorption	specific anion ads.
PtCo/C (Pt and Co-OH at surface)	little anion adsorption	site-specific anion ads.
PtFe/C (Pt skin)	little anion adsorption	specific anion ads and perhaps rearrangement of Pt skin

Figure 9 demonstrates that $\Delta\mu$ for Pt/C and Pt_3Fe/C nanoparticles reflects a negative Pt−Pt scattering (i.e., $-\delta$(Pt−Pt)) below 50 eV while the Pt_3Co/C alloy shows perhaps some $-\delta$(Pt−Pt) EXAFS scattering but also significant Pt−O scattering, the latter suggestive of O in bridge/fcc sites by comparison with the theoretical signatures in Figure 1. Table 2 summarizes the circumstances which can explain this data. At 0.6 V, insignificant OH should be adsorbed, so the anions are just specifically adsorbed on the Pt both in Pt/C and Pt_3Fe/C. On the other hand, when Co−O(H) exists at the surface, lateral interactions again force the anions to site-specifically adsorb so that they are visible in $\Delta\mu$. Thus, both OH adsorption on pure Pt at 0.74 V or Co−O(H) sites on the Pt_3Co/C even at 0.6 V force the anions into site-specific registry on the surface.

$\Delta\mu$ for both Pt/C and Pt_3Fe/C in Figure 9 exhibits $-\delta$(Pt−Pt) EXAFS scattering below 50 eV as discussed; however, the magnitude for the PtFe alloy is nearly 10−20 times larger than that for pure Pt. What can cause this dramatic increase for the alloy? The electronic effect from the subsurface Fe could increase the Pt−anion interaction and therefore weaken the Pt−Pt bond more significantly, thus strongly decreasing the short-range Pt−Pt EXAFS scattering. Current−voltage curves for the Pt_3Fe/C alloy show almost no peak due to O(H) adsorption, suggesting that the TFMSA anion adsorption could indeed be so strong as to completely hinder O(H) chemisorption. However, we are still a bit surprised by the nearly 20-fold increase in the $-\delta$(Pt−Pt) magnitude for the Fe alloy compared to pure Pt. This very large magnitude could also be caused in part by a rearrangement of the Fe atoms within the nanoparticle, i.e., the specific anion adsorption in the 6 M TFMSA could cause the Pt skin to grow thicker, thus changing N_{Pt-Pt} relative to N_{Pt-Fe}. We note that if more Fe leached out in the stronger 6 M compared to the 1 M TFMSA, the reverse would be observed, i.e., N_{Pt-Pt} would increase. Clearly more work is required to fully understand the alloying effect on the anion adsorption, but the above results clearly suggest it is a strong affect and depends critically on whether a Pt skin exists or not.

Conclusions

As summarized in the Introduction, adsorption of anions from the electrolyte either blocks or "crowds" available adsorption sites and changes the electronic and/or geometric properties of the Pt nanoparticles. We have seen evidence for all of these effects. More specifically, we have seen the following. (1) Significant specific anion adsorption occurs in 0.1 M H_2SO_4 and 6 M TFMSA, while it does not in 0.1 M $HClO_4$ and 1 M TFMSA. (2) Specific anion adsorption significantly hinders O(H) adsorption, particularly formation of subsurface O. (3) Specific anion adsorption causes the Pt nanoparticle to become more spherical to increase exposure to the electrolyte and weakens Pt−Pt bonding at the surface. (4) The specific anion adsorption becomes site specific only after lateral interactions from other chemisorbed species at the surface force the anions to go into specific adsorption sites (see Table 1). (5) The effect of alloying appears to have a profound affect on the strength of the anion adsorption, and the morphology determines whether site-specific or just specific adsorption occurs (See Table 2). These results show that in situ XANES can provide detailed information on specific contact anion adsorption, the effect that this adsorption has on the Pt nanoparticle itself, and the chemisorption of O(H) and oxidation of the particle. Since these effects can cause profound changes in the reactivity of a fuel cell, such studies should ultimately be performed in situ on an operating fuel cell. Further, the effects of other anions, such as the halides, could easily be studied; such studies are currently in progress.[96]

Acknowledgment. The authors (S.M. and V.S.M.) express their appreciation to the Army Research Office for financial support and to the Department of Energy, Materials Science Division, for their support in building and maintaining the National Synchrotron Light Source at Brookhaven National Laboratory (BNL, Upton, NY).

References and Notes

(1) Teliska, M.; Murthi, V. S.; Mukerjee, S.; Ramaker, D. E. *J. Electrochem. Soc.* **2005**, *152A*, 2159 and references therein.
(2) Grahame, D. C. *Chem. Rev.* **1947**, *41* (3), 441−501.
(3) Trasatti, S.; Parsons, R. *J. Electroanal. Chem.* **1986**, *205*, 359.
(4) *Adsorption of Molecules at Metal Electrodes*; Lipkowski, J., Ross, P. N., Eds.; VNC Publishers: New York, 1991.
(5) Weaver, J.; Gao, X. *Annu. Rev. Phys. Chem.* **1993**, *44*, 459.
(6) Herrero, E.; Franaszczuk, K.; Wieckowski, A. *J. Phys. Chem.* **1994**, *98*, 5074.
(7) Markovic, N. M.; Ross, P. N. *Surf. Sci. Rep.* **2002**, *45*, 117.
(8) Damjanovic, A.; Brusic, V. *Electrochim. Acta* **1967**, *12*, 615.
(9) Lamy-Pitara, E.; El Mouadid, S.; Barbier, J. *Electrochim. Acta* **2000**, *45*, 4299.
(10) Zolfaghari, A.; Jerkiewicz, G. *J. Electroanal. Chem.* **1999**, *467*, 177.
(11) Horanyi, G. *Rev. Anal Chem.* **1995**, *14* (1), 58.
(12) Horanyi, G. In *A Special Periodical Report: Catalysis*; Spivey, J. J., Ed.; The Royal Society of Chemistry: Cambridge, 1996; Vol. 12, pp 254−301.
(13) Bockris, J. O. M.; Gamboa, M.; Aldeco, M.; Szklarczyk, M. *J. Electroanal. Chem.* **1990**, *339*, 3410.
(14) Zelanay, P.; Habib, M. A.; Bockris, J. O. M. *Langmuir* **1986**, *2*, 393.
(15) Jaaf-Golze, K. A.; Kolb, D. M.; Scherson, D. *J. Electroanal. Chem. Interfacial Electrochem.* **1986**, *200*, 353.
(16) Motoo, S.; Furuya, N. *Ber. Bunsen-Ges. Phys. Chem.* **1987**, *91*, 457.
(17) Clavilier, J.; Achi, K. E.; Rodes, A. *Chem. Phys.* **1990**, *141*, 1.
(18) Rodes, A.; El Achi, K.; Zamakhchari, M. A.; Clavilier, J. *J. Electroanal. Chem. Interfacial Electrochem.* **1990**, *284*, 245.
(19) Markovic, N. M.; Marinkovic, N. S.; Adzic, R. R. *J. Electroanal. Chem. Interfacial Electrochem.* **1988**, *241*, 309.
(20) Mostany, J.; Herrero, E.; Feliu, J. M.; Lipkowski, J. *J. Phys. Chem. B* **2002**, *106* (49), 12787.
(21) Savich, W.; Sun, S.; Lipkowski, J.; Wieckowski, A. *J. Electroanal. Chem.* **1995**, *338*, 233.
(22) Thomas, S.; Sung, Y. E.; Kim, H. S.; Wieckowski, A. *J. Phys. Chem.* **1996**, *100*, 11726.
(23) Clavilier, J.; Rhodes, A.; El Achi, K.; Zamakhchari, M. A. *J. Chim. Phys.* **1991**, *88*, 1291.
(24) Gomez, R.; Climent, V.; Feliu, J. M.; Weaver, M. J. *J. Phys. Chem. B* **2000**, *104*, 597.
(25) Herrero, E.; Mostany, J.; Feliu, J. M.; Lipkowski, J. *J. Electroanal. Chem.* **2002**, *534*, 79.
(26) Adzic, R. R.; Feddrix, R. R.; Nikolic, F.; Yeager, E. *J. Electroanal. Chem.* **1992**, *341*, 287.
(27) Savich, W.; Sun, S. G.; Lipkowski, J.; Wieckowski, A. *J. Electroanal. Chem.* **1995**, *388*, 233.
(28) Nart, F. C.; Iwasita, T.; Weber, M. *Electrochim. Acta* **1994**, *39*, 961.
(29) Iwasita, T.; Nart, F. C. *J. Electroanal. Chem.* **1990**, *295*, 215.
(30) Iwasita, T.; Nart, F. C.; Rodes, A.; Pastor, E.; Weber, M. *Electrochim. Acta* **1995**, *40*, 53.

(31) Faguy, P. W.; Markovic, N.; Adzic, R. R.; Fierro, C. A.; Yeager, E. B. *J. Electroanal. Chem.* **1990**, *289*, 245.
(32) Nart, F. C.; Iwasita, T.; Weber, M. *Electrochim. Acta* **1994**, *39*, 961.
(33) Sawarti, Y.; Inukai, J.; Ito, J. *J. Electron Spectrosc. Relat. Phenom.* **1993**, *64/65*, 515.
(34) Kunimatsu, K.; Samant, M. G.; Seki, H. *J. Electroanal. Chem.* **1988**, *258*, 163.
(35) Kunimatsu, K; Samant, M. G.; Seki, H. *J. Electroanal. Chem.* **1988**, *243*, 203.
(36) Shinggaya, Y.; Ito, M. *J. Electroanal. Chem.* **1990**, *295*, 215.
(37) Iwasita, T.; Nart, F. C.; Rodes, A.; Pastor, E.; Weber, M. *Electrochim. Acta* **1995**, *40*, 53.
(38) Faguy, P. W.; Marinkovic, N. S.; Adzic, R. R. *J. Electroanal. Chem.* **1996**, *407*, 209.
(39) Faguy, P. W.; Marinkovic, N. S.; Adzic, R. R. *Langmuir* **1996**, *12*, 243.
(40) Nart, F. C.; Iwasita, T.; Weber, M. *Electrochim. Acta* **1994**, *39*, 961.
(41) Wieckowski, A. In *Modern Aspects of Electrochemistry*; Bockris, J. O. M., Conway, B. E., White, R. E., Eds.; Plenum Press: New York, 1990; Vol. 21, p 65.
(42) Zelenay, P.; Wieckowski, A. In *Electrochemical Interfaces: Modern Techniques for In Situ Surface Characterization*; Abruna, H. D., Ed.; VCH Publishers: New York, 1991; p 479.
(43) Kolics, A.; Wieckowski, A. *J. Phys. Chem.* **2001**, *105*, 2588.
(44) Gamboa-Aldeco, M. E.; Franaszczuk, K.; Wieckowski, A. In *The Handbook of Surface Imaging and Visualization*, lst ed.; Hubbard, A. T., Ed.; CRC Press: New York, 1995; p 635.
(45) Sung, Y. E.; Thomas, A.; Gamboa Aldeco, M.; Franaszczuk, K.; Wieckowski, A. *J. Electroanal. Chem.* **1994**, *378*, 131.
(46) Wieckowski, A.; Zelenay, P.; Varga, K. *J. Chem. Phys.* **1991**, *88*, 1247.
(47) Gamboa-Aldeco, M. E.; Herreo, E.; Zelanay, P. S.; Wieckowski, A. *J. Electroanal. Chem.* **1993**, *348*, 451.
(48) Gamboa-Aldeco, M. E.; Herrero, E.; Zelenay, P. S.; Wieckowski, A. *J. Electroanal. Chem.* **1993**, *348*, 451.
(49) Thomas, S.; Sung, Y. E.; Kim, H. S.; Wieckowski, A. *J. Phys. Chem.* **1996**, *100*, 11726.
(50) Funtikov, A. M.; Stimming, U.; Vogel, R. *J. Electroanal. Chem.* **1997**, *428*, 147.
(51) Lachenwitzer, A.; Li, N.; Lipkowski J. *J. Electroanal. Chem.* **2002**, *532*, 85.
(52) Faguy, P. W.; Markovic, N. M.; Adzic, R. R.; Fierro, C. A.; Yeager, E. B. *J. Electroanal. Chem.* **1992**, *330*, 433.
(53) Gamboa-Aldeco, M. E.; Hererro, E.; Zelanay, P.; Wieckowski, A. *J. Electroanal. Chem.* **1993**, *348*, 451.
(54) Perez, J.; Villullas, H. M.; Gonzalez, E. R. *J. Electroanal. Chem.* **1997**, *435*, 179.
(55) Markovic, N. M.; Adzic, R. R.; Cahan, B. D.; Yeager, E. B. *J. Electroanal. Chem.* **1994**, *377*, 249.
(56) Mrozek, P.; Sung, Y. E.; Wieckowski, A. *Surf. Sci.* **1995**, *335*, 44.
(57) Yau, S. L.; Kim, Y. G.; Itaya, K. *J. Am. Chem. Soc.* **1996**, *118*, 7795.
(58) Calvente, J. J.; Marinkovic, N. S.; Kovascova, Z.; Fawcett, W. R. *J. Electroanal. Chem.* **1997**, *421*, 49.
(59) Smirnov, P.; Wakita, H.; Yamaguchi, T. *J. Phys. Chem. B* **1998**, *102*, 4802.
(60) Nakamoto, K. *Infrared and Raman Spectra of Inorganic and Coordination Compounds*, 5th ed.; Wiley: New York, 1997 and references therein.
(61) Baranska, H.; Labudzinska, A.; Terpinski, A. *Laser Raman Spectrometry*; Horwood: Chichester, 1987.
(62) Zheng, W.; Tadjeddine, A. *J. Chem. Phys.* **2003**, *119* (24), 13096.
(63) Olivera, P. P.; Parito, M.; Sellers, H. Electronic structure calculations of polyatomic oxyanions adsorbed on metal surfaces. In *Interfacial Electrochemistry*; Wieckowski, A., Ed.; Marcel-Dekker: New York, 1999; p 63.
(64) Hsueh, K. L.; Gonzalez, E. R.; Srinivasan, S. *Electrochim. Acta* **1983**, *28*, 691.
(65) Appleby, A. J.; Baker, B. S. *J. Electrochem. Soc.* **1978**, *125*, 404.
(66) O'Grady, W. E.; Taylor, E. J.; Srinivasan, S. *J. Electroanal. Chem.* **1982**, *132*, 137.
(67) Gonzalez, E. R.; Srinivasan, S. *Electrochim. Acta* **1982**, *27*, 1425.
(68) Habib, M. A.; Bockris, J. O. M. *J. Electrochem. Soc.* **1983**, *130* (12), 2510.
(69) Enayetullah, M. A.; DeVilbiss, T. D.; Bockris, J. O. M. *J. Electrochem. Soc.* **1989**, *136*, 3369.
(70) Murthi, V. S.; Urian, R. C.; Mukerjee, S. *J. Phys. Chem. B* **2004**, *108* (30), 11011−11023.
(71) Koetz, R.; Clouser, S.; Sarangapani, S.; Yeager, E. *J. Electrochem. Soc.* **1984**, *131*, 1097.
(72) Conway B. E.; Novak, D. M. *J. Electrochem. Soc.* **1981**, *128*, 956.
(73) Zelanay, P. S.; Habib, M. A.; Bockris, J. O. M. *J. Electrochem. Soc.* **1984**, *131*, 2464.
(74) Zelanay, P. S.; Rhee, C.; Mrozek, P.; Wieckowski, A. *39th National Symposium of the American Vacuum Society*, Chicago, 1992; Abstract 365.
(75) Zinola, C. F.; Castro Luna, A. M.; Triaca, W. E.; Arvia, A. J. *J. Electrochem. Soc.* **1987**, *134*, 1135.
(76) Jalan, V. M.; Bushnell, C. L. (United Technologies Corp.). Highly Dispersed Catalytic Platinum. U.S. Patent 4,137,379, 1979.
(77) Jalan, V. M. (Giner, Inc.). Cathode Alloy Electrocatalysts. Eur. Patent 55079197, 1985.
(78) Landsman D. A.; Luczak, F. J. (United Technologies Corp.). Precious Metal-Chromium Alloy Catalyst for Fuel Cell Electrodes. Belg. Patent 4,373,014, 1981.
(79) Stonehart, P.; Watanabe, M.; Yamamoto, N.; Nakamura, T.; Hara, N.; Tsurumi, K. (Stonehart Associates Inc.). Platinum Alloy Electrode Catalyst. Jpn. Kokai Tokkyo Koho. 5,225,391, 1992.
(80) Mukerjee, S.; Srinivasan, S.; Soraigo, M.; McBreen, J. *J. Phys. Chem.* **1995**, *99*, 4577. Mukerjee, S.; Srinivasan, S.; Soraiga, M. *J. Electrochem. Soc.* **1995**, *142*, 1409.
(81) Parthasarathy, A.; Brumlik, C. J.; Martin, C. R. *Polym. Mater. Sci. Eng.* **1993**, *68*, 117.
(82) Holdcroft, S.; Abdou, M. S.; Beattie, P.; Basura, V. Ultramicroelectrode studies of oxygen reduction in polyelectrolyte membranes. In *New Materials for Fuel Cell and Modern Battery Systems II*, Proceedings of the 2nd International Symposium on New Materials for Fuel Cell and Modern Battery Systems, Montréal, Canada, July 6−10, 1997; Savadogo, O., Roberge, P. R., Eds.; Editions de l'Ecole Polytechnique de Montréal: Montreal, Canada, 1997; p 863.
(83) McBreen, J. *Phys. Electrochem.* **1995**, 339.
(84) Koningsberger, D. C.; de Graaf, J.; Mojet, B. L.; Ramaker, D. E.; Miller, J. T. *Appl. Catal.* **2000**, *191*, 205.
(85) Mojet, B. L.; Miller, J. T.; Ramaker, D. E.; Koningsberger, D. C. *J. Catal.* **1999**, *186*, 373.
(86) Ramaker, D. E.; Mojet, B. L.; Garriga Oostenbrink, M. T.; Miller, J. T.; Koningsberger, D. C. *Phys. Chem. Chem. Phys.* **1999**, *1*, 2293.
(87) Koningsberger, D. C.; Oudenhuijzen, M. K.; Bitter, J. H.; Ramaker, D. E. *Top. Catal.* **2000**, *10*, 167.
(88) Mojet, B. L.; Ramaker, D. E.; Miller, J. T.; Koningsberger, D. C. *Catal. Lett.* **1999**, *62*, 15.
(89) Teliska, M.; O'Grady, W. E.; Ramaker, D. E. *J. Phys. Chem. B* **2004**, *108*, 2333.
(90) Teliska, M.; O'Grady, W. E.; Ramaker, D. E. *J. Phys. Chem. B* **2005**, *109*, 8076.
(91) Roth, C.; Martz, N.; Buhrmester, T.; Mazurek, M.; Loster, M.; Koningsberger, D. C.; Ramaker, D. E.; Fuess, H. *J. Am. Chem. Soc.* **2005**, *127*, 14607.
(92) Scott, F. J.; Mukerjee, S.; Ramaker, D. E. *J. Electrochemical Soc.* **2007**, *154*, A396.
(93) Janin, E.; von Schenck, H.; Gothelid, M.; Karlsson, U. O. *Phys. Rev. B* **2000**, *61*, 13144.
(94) Ankudinov, A. L.; Ravel, B.; Rehr, J. J.; Bare, S. *Phys. Rev. B* **1998**, *58*, 7565.
(95) Sung, Y. E.; Chrzanowski, W.; Zolfaghari, A.; Jerkiewicz, G.; Wieckowski, A. *J. Am. Chem. Soc.* **1997**, *119*, 194−200.
(96) Arruda T.; Ziegelbauer, J. M.; Mukerjee S.; Gatewood, D.; Shyam, B.; Ramaker, D. E. Unpublished results.